6. In the range of the variables investigated, an increase in flow rate is detrimental to oil-mass formation and propagation. The data may be correlated by plotting the increase in oil recovery as a function of the ratio of the flow rate to the square root of the permeability (essentially the ratio of the hydraulic forces to the capillary forces).

ACKNOWLEDGMENT

Financial assistance from the American Petroleum Institute (A.P.I Grant in Aid No. 97) is gratefully acknowledged. The advice, guidance, and suggestions of Dr. F. M. Perkins, Jr., and later Dr. C. W. Arnold of Humble Oil and Refining Company, A.P.I. Liaison Representatives for this project, and of Dr. R. O. Leach of Pan American Petroleum Corp. are deeply appreciated. The glass-grid micromodel was courteously provided by Dr. C. C. Mattax who was responsible for its design and construction.

NOTATION

k = hydraulic permeability, darcies
ΔP = pressure drop across column, lb./sq. in.
P.V. = pore volume, ml.
ΔR = increase in oil recovery relative to an untreated water-oil displacement, % pore volume
r = average pore radius, μ
U_x = velocity of oil perpendicular to direction of flow, ft./day
U_y = velocity of oil in direction of flow, ft./day
V = flow rate, ft./day
γ_{ow} = oil-water interfacial tension, dynes/cm.
μ_o = viscosity of oil phase at 35°C., centipoises
μ_w = viscosity of water phase at 35°C., centipoises
θ = contact angle (viewed through aqueous phase), deg.

LITERATURE CITED

1. Caro, R. A., J. C. Calhoun, and R. F. Nielsen, *Oil Gas J.*, **51**, 62 (1952).
2. Johansen, R. T., N. H. Dunning, and J. W. Beaty, *Penn. State Univ. Mineral Ind. Exp. Sta. Bull. 68* (1955).
3. Kyte, J. R., and L. A. Rapoport, Am. Inst. Mining Engrs., Preprint No. 929G, Dallas, Texas (October, 1957).
4. Leach, R. O., O. R. Wagner, H. W. Wood, and C. F. Harpke, *J. Petrol. Technol.*, **14**, 206 (1962).
5. Mattax, C. C., and J. R. Kyte, *Oil Gas J.*, **59**, 42 (1961).
6. Michaels, A. S., and R. S. Timmins, *Trans. Am. Inst. Mining Engrs.*, **219**, 150 (1960).
7. Stahl, C. D., J. C. Calhoun, F. W. Preson, and R. F. Nielsen, *Penn. State Univ. Minerals Ind. Exp. Sta. Bull. 59* (1951).
8. Stancell, A., Sc.D. thesis, Mass. Inst. Technol., Cambridge, Massachusetts (1962).
9. Taber, J. J., *Trans. Am. Inst. Mining Engrs.*, **213**, 186 (1958).
10. Timins, R. S., Sc.D. thesis, Mass. Inst. Technol., Cambridge, Massachusetts (1959).
11. Torrey, P. D., "Evaluation of Secondary Recovery Prospects," Economics of Petroleum Exploration, Development, and Property Evaluation, Prentis Hall, Englewood Cliffs, New Jersey (1961).
12. Wagner, O. R., and R. O. Leach, *Trans. Am. Inst. Mining Engrs.*, **216**, 65 (1959).

Manuscript received June 30, 1964; revision received December 29, 1964; paper accepted January 13, 1965. Paper presented at A.I.Ch.E. Pittsburgh meeting.

Local Parameters in Cocurrent Mercury-Nitrogen Flow: Parts I and II

L. G. NEAL and S. G. BANKOFF

Northwestern University, Evanston, Illinois

An experimental study was made in a cocurrent vertical mercury-nitrogen flow of local parameters, including local liquid velocity and gas fraction. In Part I the pertinent quantities are carefully defined and power-law continuity expressions derived. A description is given of the apparatus, including a simple local liquid velocity probe. In Part II experimental velocity and void profiles are given for the mercury-nitrogen flow. The regime is slug flow, but the slugs are not axisymmetrical, on account of the nonwetted walls. Intensities of density and liquid velocity fluctuations are computed for the first time and a comparison made with Levy's mixing-length theory.

PART I

Because of their attractiveness in the design of compact power plants, considerable attention has been focussed recently on the mechanics of cocurrent flows in pipes or channels of a liquid metal and a gaseous phase. In some ways, these flows exhibit unique features not found to such a pronounced degree in two-phase flows involving the usual aqueous or organic media. For example, because of the high surface energy and density of liquid metals, the slug flow regime normally prevails. Except in special circumstances, moreover, the gas concentrates at the walls of the pipe, owing to the poor wetting properties of liquid metals in contact with most engineering surfaces. This gives rise to asymmetric (frequently helicoidal) gas slugs which hug the pipe wall, in contrast to the axisymmetric slugs observed in aqueous flows.

L. G. Neal is with the TRW Space Technology Laboratories, Redondo Beach, California.

Apart from their inherent interest, however, liquid metal two-phase flows exhibit some properties which make them uniquely suited for investigation of the fine structure of liquid-gas flows. For one thing, the high electrical conductivity and surface energy of liquid metals are favorable for the application of a resistivity probe to detect the presence or absence of liquid at a particular point in the flow (*1*). A simple circuit design allows detection of a bubble of the order of 0.1-in. diam. in a mercury-nitrogen flow, whereby the void fraction and bubble frequency can be determined as functions of radial and axial position. In addition, the high liquid density makes the measurement of time-average momentum flux at a particular location feasible, with the use of an impact probe. Detailed measurements of this sort have not been previously available in slug or bubble flow.

The advent of these measuring techniques makes it advisable to define the mean and fluctuating parameters in two-phase flow more precisely than has heretofore been necessary. In analyzing the data it will be convenient to represent the mean velocity and void fraction profiles as power-law functions of the distance from the wall. This is similar to an earlier treatment (*2*) of well-dispersed two-phase flows, where the effects of local slip were neglected. This is not permissible in the present case, and a suitable modification of the material balance equation is developed. These preliminaries having been disposed of, the major portion of this study deals with vertical cocurrent mercury-nitrogen flow in a 1-in. stainless steel pipe. Radial velocity and void fraction data are obtained and correlated in terms of empirical functions of the gas volumetric flow concentration β and the Froude number, based on the superficial liquid velocity. Cross-sectional average slip velocity ratios, which are shown to be attributable almost entirely to local, rather than distributional, slip, are compared with previous measurements. In addition, typical data of bubble frequency and size distribution, together with calculated local stream density and velocity variances, are given, to the authors' knowledge, for the first time in two-phase flow. The latter quantities are of special interest in connection with Levy's mixing-length theory (*3*).

PRELIMINARY DISCUSSION

Definitions

The nature of the experimental work makes it advisable to define the two-phase flow stochastic variables with somewhat more precision than has heretofore been available. One notes first the existence of a discrete random variable $X(\mathbf{x}, t)$ which takes the value unity, or zero, depending upon whether liquid or gas is present at the point denoted by the position vector $\mathbf{x}$ at the time t. Denote by $P[X(\mathbf{x}, t)]$ the probability that $X = 1$ at a particular point in space and time. This implies that one examines the results of a large number of experiments with identical initial and boundary conditions. This is rarely convenient, and some sort of averaging procedure based upon a single experiment is clearly preferable.*

One can define a nondenumerable infinity of expected-value operators; the authors will, however, confine their attention to the two most important. The time-average operator E_t denoted by an overscore is

$$E_t[X] = \frac{1}{T}\int_{-T/2}^{T/2} X(\mathbf{x}, t+\tau)\,d\tau = \overline{X}(\mathbf{x}, t) \qquad (1)$$

where T is a time interval chosen to be large compared with the time scale of the fluctuating quantity. How this may be performed will presently become clear. If $\overline{X}(\mathbf{x}, t) = P[X(\mathbf{x}, t)]$ for all $\mathbf{x}$ and t, the flow is said to be quasi steady.

In conformity with usual practice, one denotes $1 - \overline{X} \equiv \alpha$, the local void fraction. Similarly, a space-average operator E_x, denoted by triangular brackets, may be defined as

$$E_x[X] = \frac{1}{V}\int_R X(\mathbf{x}+\mathbf{r}, t)\,d\mathbf{r} = \langle X(\mathbf{x}, t)\rangle \qquad (2)$$

where $\mathbf{r}$ is the positive vector from the point $\mathbf{x}$ to some neighboring point, so that $d\mathbf{r}$ is a volume element in some region, R, of volume V, surrounding the point $\mathbf{x}$. The characteristic dimension of the region R should likewise be chosen to be large compared with the length scale of the fluctuating quantity. If $\langle X(\mathbf{x}, t)\rangle = P[\overline{X}(\mathbf{x}, t)]$ for all $\mathbf{x}$ and t, the flow field is said to be homogeneous. In determining the space-average value of a random variable at a point, the region R is conveniently chosen to be a sphere centered at the point. By analogy, one may write $\langle 1 - X\rangle \equiv \xi$, the instantaneous spatial void fraction. By the commutativity of the expected-value operators, $\langle\alpha\rangle = \overline{\xi}$.

For nonhomogeneous flows, the expected value will depend upon the dimensions of the region R. Frequently one wishes to obtain the cross-sectional average value of a nonhomogeneous flow, in which case the region R is a thin, disk shaped volume spanning the flow, and $\langle X\rangle$ is determined by the axial position variable and the time.

The time-average frequency with which the random variable fluctuates may now be written as

$$E_t\left[\frac{1}{2}\left|\frac{\partial X}{\partial t}\right|\right] = \frac{1}{T}\int_{-T/2}^{T/2}\left|\frac{\partial X(\mathbf{x}, t+\tau)}{\partial t}\right| d\tau = \frac{N(t)}{T} = F \qquad (3)$$

where N is the number of bubbles passing through the point $\mathbf{x}$ in the time interval $(t - T/2, t + T/2)$, and F is an average frequency for that interval. Since the integrand consists of a sequence of delta functions, a Stieltjes integral is understood. T is to be chosen so that $N >> 1$, or $T >> 1/F$. Similarly, one can define a space-average wave number (or average bubble spacing) by

$$E_{x_1}\left[\frac{1}{2}\left|\frac{\partial X}{\partial x_1}\right|\right] = \frac{1}{L}\int_{-L/2}^{L/2}\left|\frac{\partial X(x_1 + r_1, x_2, x_3, t)}{\partial x_1}\right| dr_1 = \frac{N_1(\mathbf{x})}{L} = m \qquad (4)$$

where the integration is performed along a line of length L in the x_1 direction centered at the point $\underline{x}$. The choice for the x_1 direction is arbitrary, and, in general, different directions will lead to different average spacings. Analogously, L is to be chosen so that $N >> 1$. Extensions of the averaging process to more than one dimension are immediate.

One can similarly discuss the central moments of the random variable, X. Denoting the moments of order one

* It may seem to the practicing design engineer that the definitions to follow are unnecessarily formal and cumbersome. In fact, however, they are necessary to treat the unsteady aspects of two-phase flows with sufficient rigor. One example will be given later in discussing a recently proposed mixing-length theory for two-phase flows (*3*). Another area of considerable current interest is the propagation of density disturbances in two-phase flows because of its intimate connection with reactor stability and control (*4*). A promising avenue of attack is the kinematic wave concept introduced by Lighthill and Whitham (*5*) in connection with flood waves on rivers and traffic waves on a crowded highway and applied to two-phase flows by Zuber (*6*) and Wallis (*7*). The problem arises, from a practical point of view, of how one is to define the gas concentration at points near the wave front. For periodic disturbances, one can define an expected-value operator whose effect is to average over a large number of samples taken at a particular phase angle with reference to the input disturbance. Such an averaging procedure is evidently quite different from those discussed above.

for any expected-value operator by $m = E(X)$, the variance is given by $\sigma^2 = E[(X-m)^2]$. For quasi steady flows, the root-mean-square void fraction fluctuation is therefore defined by

$$\tilde{\alpha} = [E_t((1-X-\alpha)^2)]^{1/2} \tag{5}$$

where $\tilde{\alpha} = \tilde{\alpha}(\mathbf{x})$.

The velocity of the stream at a particular point in time and space is likewise a stochastic vector function: $\mathbf{U} = \mathbf{U}(\mathbf{x}, t)$. One can define an average liquid velocity, in general, as $E(X\mathbf{U})/E(X)$, with a corresponding definition for the gas velocity. For a quasi steady flow this implies

$$\mathbf{U}_L(\mathbf{x}) = \frac{E_t(X\mathbf{U})}{E_t(X)} = \frac{1}{T(1-\alpha)} \int_{-T/2}^{T/2} X(\mathbf{x}, \tau)\, \mathbf{U}(\mathbf{x}, \tau)\, d\tau \tag{6}$$

The numerator corresponds to a time-average local superficial velocity:

$$\overline{\mathbf{U}}_{sL}(\mathbf{x}) = (1-\alpha)\, \overline{\mathbf{U}}_L(\mathbf{x}) \tag{7}$$

When one denotes by the brevet superscript the space-averaging process over the flow cross-section of area A, the corresponding expressions are

$$\hat{\mathbf{U}}_L = \frac{\hat{X\mathbf{U}}}{\hat{X}} = \frac{\frac{1}{A}\int_A X\mathbf{U} \cdot d\mathbf{A}}{1-\zeta} \tag{8}$$

The instantaneous cross-sectional average superficial velocity follows immediately:

$$\hat{\mathbf{U}}_{sL}(t) = (1-\zeta)\, \hat{\mathbf{U}}_L(t) \tag{9}$$

One can write corresponding expressions for the average gas velocities. The well-known relationship between the mixture velocity $\overline{U}$ and the average gas and liquid velocities follows immediately from the definition of the time-average gas velocity:

$$\mathbf{U}_G(\mathbf{x}) = \frac{E_t[(1-X)\mathbf{U}]}{E_t(1-X)} = \frac{\mathbf{U} - \mathbf{U}_L(1-\alpha)}{\alpha} \tag{10}$$

The density is also a stochastic variable of space and time, given by

$$\rho = \rho(\mathbf{x}, t) = \rho_L X + \rho_G\,(1-X);\ \rho_G = \overline{\rho}_G + \rho_G' \tag{11}$$

where the liquid density may be considered to be constant, but the gas density, strictly speaking, is a stochastic function of space and time, due to turbulent pressure fluctuations. When one assumes either that the gas density fluctuations are small, or that they are uncorrelated with the random variable X, or both, application of the time-averaging operator to Equation (11) yields the familiar expression

$$\overline{\rho} = \rho_L\,(1-\alpha) + \overline{\rho}_G\alpha \tag{12}$$

The root-mean-square velocity fluctuation is a scalar quantity defined by

$$\tilde{U} = [E_t((\mathbf{U}-\overline{\mathbf{U}})^2)]^{1/2} = [E_t(\mathbf{U}'^2)]^{1/2} \tag{13}$$

where $\mathbf{U}'$ is the instantaneous fluctuation of the stream velocity. The stream velocity itself is a stochastic variable given by

$$\mathbf{U} = \mathbf{U}_L X + \mathbf{U}_G\,(1-X);\ \mathbf{U}_L = \overline{\mathbf{U}}_L + \mathbf{U}_L' \tag{14}$$

with an analogous definition for the turbulent gas velocity fluctuation $\mathbf{U}_G'$. The application of the second central moment operator to the density at a particular point in a quasi steady flow likewise gives

$$\tilde{\rho} = [E_t((\overline{\rho}-\rho)^2)]^{1/2} = (\overline{\rho^2} - \overline{\rho}^2)^{1/2} \tag{15}$$

Similarly, the instantaneous fluctuation of the stream velocity is given from Equations (10) and (14) by

$$\mathbf{U}' \equiv \mathbf{U} - \overline{\mathbf{U}} = \mathbf{U}_L\,(X-1+\alpha) + \overline{\mathbf{U}}_G(1-X-\alpha) + \mathbf{U}_L'X + \mathbf{U}_G'\,(1-X) = (\overline{\mathbf{U}}_L - \overline{\mathbf{U}}_G)\,(X-1+\alpha) + \mathbf{U}_L'X + \mathbf{U}_G'\,(1-X) \tag{16}$$

One notes that $X^2 = X$, so that

$$\overline{(X-1+\alpha)^2} = \overline{X}^2 - 2(1-\alpha)\overline{X} + (1-\alpha)^2 = (1-\alpha)\alpha \tag{17}$$

Also, the assumption that the turbulent velocity fluctuations are uncorrelated with the stochastic phase variable X implies $\overline{\mathbf{U}_L'X} = \overline{\mathbf{U}_G'X} = 0$. When one notes finally that $X(1-X) = 0$, it follows that

$$\tilde{U}^2 = \overline{\mathbf{U}'^2} = (\overline{\mathbf{U}}_G - \overline{\mathbf{U}}_L)^2\alpha(1-\alpha) + \overline{\mathbf{U}_L'^2}(1-\alpha) + \overline{\mathbf{U}_G'^2}\alpha \tag{18}$$

This states that the mean-square velocity fluctuation is the sum of the contributions due to the alternating presence of gas and liquid and to the turbulent liquid and gaseous velocity fluctuations. If the local slip ratio is unity, corresponding to equal mean velocities of the two phases, the first term vanishes, as it should. For many cases of bubble or froth flow, therefore, the last two terms on the right side of Equation (18) cannot be neglected. In the present work, however, it will be shown that local slip is quite large, so that it seems reasonable to neglect these terms. With this assumption the root-mean-square velocity fluctuation becomes

$$\tilde{U} = [(\overline{\mathbf{U}}_G - \overline{\mathbf{U}}_L)^2\alpha(1-\alpha)]^{1/2} \tag{19}$$

Similarly, the density variance for a quasi steady flow turns out to be

$$\tilde{\rho}^2 = (\rho_L - \overline{\rho}_G)\,(1-\alpha)\,\alpha + \tilde{\rho}_G^2\alpha \tag{20}$$

where the contribution of the turbulent density fluctuation of the gas, given by the last term on the right-hand side, can in almost all cases be neglected.

One can similarly define covariances, or cross correlations between the fluctuating quantities:

$$\overline{\rho'\mathbf{U}'} = \overline{\{[(\rho_L - \overline{\rho}_G)\,(X-1+\alpha) + \rho_G'(1-X)] \times [(\overline{\mathbf{U}}_L - \overline{\mathbf{U}}_G)\,(X-1+\alpha) + \mathbf{U}_L'X + \mathbf{U}_G'(1-X)]\}} = (\rho_L - \rho_G)\,(\overline{\mathbf{U}}_L - \overline{\mathbf{U}}_G)\alpha(1-\alpha) + \overline{\rho_G'\mathbf{U}_G'}\,\alpha \tag{21}$$

Generally the last term on the right will again be negligible. This equation implies that the covariance is negative for vertical upward cocurrent flow and positive for downward flow. For horizontal flow, or homogeneous (froth, bubble, or mist) flow, where the two phases move at the same velocity, the first term vanishes, and the covariance is nearly zero. This illustrates the strong influence of the flow regime on the fluctuating quantities.

Intensities for the velocity and density fluctuations, analogous to the corresponding concepts in single-phase turbulent flow, may also be defined:

$$\frac{\widetilde{U}}{|\overline{U}|} = \frac{[(\overline{U}_G - \overline{U}_L)^2\alpha(1-\alpha)]^{1/2}}{|\overline{U}_G\alpha + \overline{U}_L(1-\alpha)|} \quad (22)$$

$$\frac{\widetilde{\rho}}{\rho} = \frac{[(\rho_L - \rho_G)^2(1-\alpha)\alpha]^{1/2}}{\rho_L - (\rho_L - \overline{\rho}_G)\alpha} \quad (23)$$

The covariance can similarly be made dimensionless:

$$\frac{\overline{\rho' U'}}{|\overline{\rho}\overline{U}|} = \frac{(\rho_L - \overline{\rho}_G)(\overline{U}_L - \overline{U}_G)\alpha(1-\alpha)}{|[(\overline{\rho}_G - \rho_L)\alpha + \rho_L][(\overline{U}_L - \overline{U}_G)(1-\alpha) + \overline{U}_G]|} \quad (24)$$

It should be noted that these definitions, which have been formulated for quasi steady flows in connection with the present work, may be immediately extended to other types of flows by use of the appropriate expected-value operators.

Finally, the time-mean kinetic energy of the stream is of interest in connection with the impact probe to be described:

$$\overline{\rho U^2} =$$

$$\overline{[\rho_L X + \rho_G(1-X)][(\overline{U}_L + U_L')X + (\overline{U}_G + U_G')(1-X)]^2}$$

$$= \rho_L(\overline{U}_L^2 + \widetilde{U}_L^2)(1-\alpha) + \overline{\rho_G}(\overline{U}_G^2 + \widetilde{U}_G^2)\alpha + (\overline{2\rho_G' U_G'} \cdot \overline{U}_G + \overline{\rho_G' U_G'^2})\alpha \quad (25)$$

In the present work it is permissible to neglect all but the first term on the right-hand side, so that

$$\overline{\rho U^2} \sim \rho_L(1-\alpha)(\overline{U}_L^2 + \widetilde{U}_L^2) \quad (26)$$

Material Balances

For many quasi steady two-phase flows in vertical constant-area ducts exhibiting some degree of rotational symmetry, the mean void fractions and axial phase velocities may be conveniently approximated in terms of a power law involving a suitable dimensionless distance from the wall. For a round tube the dimensionless distance is taken to be $S = 1 - r/R$, where r and R are the radial coordinate and the tube radius, respectively. Then, at a given axial position, one may write

$$\overline{U}_G^* = \overline{U}_G/\overline{U}_{GO} = S^{1/m} \quad (27)$$

$$\overline{U}_L^* = \overline{U}_L/\overline{U}_{LO} = S^{1/n} \quad (28)$$

$$\alpha^* = \frac{\alpha - \alpha_W}{\alpha_O - \alpha_W} = S^{1/p} \quad (29)$$

where α^* represents the ratio of excess void fraction at S over that at the wall to the excess void fraction at the centerline, where $\overline{U}_L^*$ and $\overline{U}_G^*$ are axial liquid and gas velocities similarly made dimensionless with respect to the corresponding quantities at the center of the tube, and where the exponents are positive, real quantities. The curvature may be positive or negative, according as the exponent is greater or less than unity, but can never change sign in the interval $O < S < 1$. Hence, profiles exhibiting either inflection or stationary points within this interval cannot be described by a single one-parameter expression of this sort, and modified expressions involving two empirical constants must be sought.

A similar problem arises in the case of nonwetting liquids. It is satisfactory to assume that both the liquid and gas velocity vanish at the tube wall, and, for wetting liquids in the absence of net gas generation at the tube wall, that the void fraction vanishes there as well. For nonwetting liquids, however, such as mercury in a stainless steel tube under ordinary conditions, or for boiling two-phase flow with heat input at the walls, the last assumption is no longer strictly valid. However, for fully-developed flows the void fraction profile frequently increases monotonically towards the center line, even in these cases, and since no direct measurement of the void fraction at the wall was possible in the present equipment because of the wall conductivity, it seems hardly justified to present a two-constant correlation. The authors have, therefore, chosen to assume that $\alpha_W = O$ for the purposes of data correlation, recognizing that well over 99% of the flow is contained in the region traversed by the probe.

Now, by definition, the time-average mass flow rates of liquid and gas and the cross-sectional average gas fraction are given by

$$W_L = 2\pi \int_0^R \rho_L \overline{U}_L(1-\alpha) r dr = 2\pi R^2 \rho_L \overline{U}_{LO}(\Omega_n - \alpha_O\Omega_{np}) \quad (30)$$

$$W_G = 2\pi \int_0^R \rho_G \alpha \overline{U}_G\, r dr = 2\pi \rho_G \overline{U}_{GO}\alpha_O\Omega_{mp} \quad (31)$$

$$\hat{\alpha} = \alpha_O\Omega_p \quad (32)$$

where use has been made of Equations (27) to (29). The constants Ω_p and Ω_{mp} are given by

$$\frac{1}{\Omega_p} = \left(\frac{1}{p} + 1\right)\left(\frac{1}{p} + 2\right) \quad (33)$$

$$\frac{1}{\Omega_{mp}} = \left(\frac{1}{m} + \frac{1}{p} + 1\right)\left(\frac{1}{m} + \frac{1}{p} + 2\right) \quad (34)$$

and the constants Ω_n and Ω_{np} are similarly defined. The cross-sectional average phase velocities are then given by

$$\hat{U}_L = \frac{\int_0^R \overline{U}_L(1-\alpha)\, r dr}{\int_0^R (1-\alpha)\, r dr} = \overline{U}_{LO}\frac{(\Omega_n - \alpha_O\Omega_{pn})}{1 - \alpha_O\Omega_p} \quad (35)$$

$$\hat{U}_G = \overline{U}_{GO}\frac{\Omega_{mp}}{\Omega_p} \quad (36)$$

The cross-sectional average slip velocity ratio and the quality are then

$$\eta = \frac{\hat{U}_G}{\hat{U}_L} = \varphi\frac{(1-\hat{\alpha})}{K - \hat{\alpha}}\delta = \varphi\delta\lambda \quad (37)$$

and

$$x = \frac{W_G}{W_G + W_L} = \left[1 + \frac{K - \hat{\alpha}}{\varphi\gamma\alpha\delta}\right]^{-1} \quad (38)$$

$$K = \frac{\Omega_p\Omega_n}{\Omega_{np}};\ \delta = \frac{\Omega_{mp}}{\Omega_{pn}};\ \varphi = \frac{\overline{U}_{GO}}{\overline{U}_{LO}};\ \text{and}\ \gamma = \frac{\overline{\rho}_G}{\rho_L} \quad (39)$$

If $m = n$, implying that the shapes of the gas and liquid velocity profiles are similar, then $\delta = 1$, and if, in addition, $\varphi = 1$, implying negligible local slip between the phases, these equations reduce to expressions given previously (2). In the present work $\varphi >> 1$, so that most of the contribution to η arises from local rather than distributional slip. On the other hand, the measured liquid velocity profiles are quite flat, so that it is probably permissible to take $\delta = 1$.

The cross-sectional average volumetric gas flow concentration β is readily found to be given by

$$\frac{\hat{\alpha}}{\beta} = \alpha\left(1 - \frac{1}{\varphi\delta}\right) + \frac{K}{\varphi\delta} \qquad (40)$$

For $\varphi\delta = 1$, this reduces to the form of the empirical equation for steam-water flow given by Armand (*8, 9*) and discussed by Zuber (*10*):

$$\hat{\alpha}/\beta = C \qquad (41)$$

on setting $C = K$. Note that C and K have separate meanings under the extended model given here, although it is not necessary that $\varphi = \delta = 1$ (only that $\varphi\delta = 1$) in order that $C = K$. This equivalence of a theoretical result based solely upon a power-law fit of the velocity and void fraction profiles and the assumption of zero local slip with an empirical relationship was a powerful argument for the negligibility of local slip at elevated pressures in steam-water flows (*2*). In the present system it will be shown that local slip is not at all negligible and in fact completely dominates distributional slip.

It may not be amiss to note that, while a considerable generalization has been achieved over the variable-density single-fluid mass balance formulation, it has been at the expense of the loss of a physically consistent model embracing both the continuity and momentum equations. As long as one does not restrict one's attention to well-dispersed flows (which implies that the wall shear stress cannot be calculated as for an idealized single-phase fluid), no regard need be given the momentum equation. The parameter K (more strictly C) can then be formulated as an empirical function of the Reynolds, Weber, and Froude numbers of the flow (*8*), as well as physical property parameters. This has been done by Hughmark (*11, 12*) in correlating slip ratios for a wide variety of gas-liquid flows and by Jones (*13, 14*) in extending the variable-density model to unsteady steam-water flows at large void fractions.

EQUIPMENT

Flow System

The general arrangement of the flow system is shown schematically in Figure 1. It consisted of a natural-circulation loop constructed of stainless steel, schedule 40 pipe. All threaded joints were sealed with a resin-base paint. Streams of C.P. grade mercury and nitrogen, metered by calibrated orifice plates, were fed to a mixing tee. The resulting two-phase mixture flowed through the test section into a separator, where the nitrogen was vented to the atmosphere and the mercury returned by gravity flow to the mixing section. In early trials air was used in place of nitrogen, but it was found that an accumulation of powdered oxides caused erratic behavior of the probes.

The test section was a 5 ft. length of 1-in. pipe, with probe and static pressure taps at five axial positions. The inlet was covered with a 150-mesh screen in order to obtain a more uniform bubble size distribution. Nevertheless, it turned out to be quite difficult to obtain a well-dispersed mercury-nitrogen entrance stream. Frequently, large pressure oscillations were observed at the lowest tap, indicating slugging at the entrance. In retrospect, it might have been desirable to install a mechanical agitator in the mixing tee in order to minimize this effect.

The static pressure was measured by stand tubes at the five points along the test section length with a maximum error of 0.1 in. Hg. The differential pressures across the orifice meters were measured with U-tube manometers filled with water for nitrogen flow and either mercury or water for mercury flow. The nitrogen supply pressure was regulated and measured by regulators and pressure

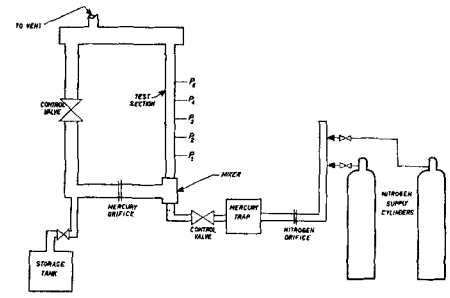

Fig. 1. Flow plan of experimental apparatus.

gauges. The temperatures of the mercury and the nitrogen were measured with iron-constantan thermocouples, with an uncertainty of ± 0.5°C. The nitrogen flow rate was controlled by two needle valves in parallel. The mercury flow rate was controlled by a 1.5-in. gate valve in the downcomer.

An instantaneous record of the presence or absence of gas at a particular point of the flow was obtained by means of a needle-shaped resistivity probe, which has been described elsewhere (*1*). The oscillograph charts were analyzed to obtain bubble frequencies, gas and liquid slug length distributions, and bubble size distributions. By feeding the probe signal into a simple integrating circuit, the local void fraction was obtained.

Local liquid velocities were obtained by means of a momentum probe, which appears to be novel and hence is described in detail below.

Impact Probe

The probe, illustrated in Figure 2, consisted of a 3 in. length of ⅛-in. stainless steel tube with one end sealed off and the other end fitted with a tubing adapter. A 1/32-in. hole was drilled in the tube wall, 3/64 in. from the closed end. The probe differs from the usual single-phase Pitot tube in at least one important respect. A Pitot tube measures the mean kinetic energy of a single-phase flow, utilizing the fact that, in the absence of friction, the dynamic pressure is constant along any streamline. The present device, however, is a momentum flux meter, which measures the time-average impulse pressure of the two-phase flow on being brought to rest in the forward direction. The instantaneous impulse pressure is given by

$$P_i = \rho U^2 (1 - \cos\theta) \qquad (42)$$

where θ, the angle of deflection of the flow immediately after contact with the probe, is nearly 90 deg. for the blunt leading edge possessed by this probe. From Equation (26) it follows that the time-average impulse pressure, to an excellent degree of approximation, is given by

$$\overline{P}_i = \rho_L (\overline{U}_L^2 + \widetilde{U}_L^2)(1 - \cos\theta)(1 - \alpha) \qquad (43)$$

When one assumes that the liquid turbulent intensity is small, this can be solved for the time-average local liquid velocity

$$\overline{U}_L = C_1[\overline{P}_i/\rho_L (1 - \alpha)]^{1/2} \qquad (44)$$

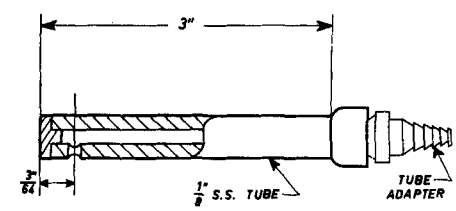

Fig. 2. Impact probe.

where corrections owing to liquid turbulence and to the nonzero probe pressure tap diameter are taken into account in the calibration constant C_1. The calibration constant was determined by graphically integrating the velocity profiles to obtain a cross-sectional average liquid velocity, which was compared with the average velocity based upon the total mass flow rate and the cross-sectional average gas fraction. Fifteen calibration runs were made over a liquid velocity range of 1.4 to 2.9 ft./sec. and $\beta = 0.17$ to 0.41. All fifteen values of the calibration constant C_1 lay in the range 0.94 to 1.00, with an average value of 0.97, demonstrating essentially complete loss of axial momentum of the liquid upon impacting the probe.

The pressure rise was thus greater by a factor of approximately 2 than in a Pitot tube, which can be explained by the following simple consideration. In a single-phase subsonic flow fluid particles on the dividing streamline begin to slow down as they approach the stagnation point, with a consequent increase in pressure which deflects the flow about the body. A two-phase flow, however, if it is suitably dispersed, acts as a succession of independent liquid masses which are not appreciably slowed down before impinging upon the body.

The static pressure signal taken at the test section wall and the impulse pressure signal were fed through ⅛ in. clear plastic pressure tubing to the bottom of two baffle filled capacitance tanks. These tanks, constructed of 12 in. lengths of 3 in. stainless steel pipe, were filled about one-third with mercury and the remainder with distilled water. This water-over-mercury arrangement served as a mechanical amplifier. The volumes of water in each leg of the system were made equal, and equal pressures were maintained at the top of each stand tube.

This arrangement overcame a major source of experimental difficulty in the probe development, which was the problem of preventing gas from entering the probe. In the early stages a differential pressure transducer was used to record the pressure signal, with the thought that a constant-volume measuring system would afford no opportunity for gas to enter the system. However, the diaphragm oscillations were sufficient to cause drift due to gas entrainment. The constant-volume system was then replaced with the constant-pressure system, which exhibited negligible drift over the time intervals of interest.

PART II

EXPERIMENTAL RESULTS AND CORRELATIONS

The parameters which were varied in this study were the mass flow rate and the relative volumes of the phases present. A natural choice of correlation groups was, therefore, a Froude number based upon the liquid superficial velocity $N_{Fr} = (\overline{U}_{SL}^2/gD_p)$ and the volumetric gas flow fraction β. The viscous forces were thought to be less important, since the Reynolds number, based upon the total mass flow rate and the mercury viscosity, was always in excess of 10^4. The following ranges of the flow variables were examined: β 0.17 to 0.93 and N_{Fr} 0.004 to 2.0.

Gas Friction and Liquid Velocity Profiles

Profiles of the gas fraction and the liquid velocity were measured at three positions along the length of the test section, measuring from the inlet at $\xi = 5.7$, 28.5, and 51.5, where the dimensionless length ξ is given as z/D_p. For many runs, an additional measurement of gas fraction was made at $\xi = 17.1$. In every case, those measurements taken at $\xi = 5.7$ exhibited entrance effects, as demonstrated by the changing profiles of both gas fraction and liquid velocity. At $\xi = 28.5$ and 51.5, the flow was always fully developed, as indicated by stable profiles, static pressure, and bubble-size spectra. The measurements at $\xi = 17.1$ showed entrance effects for small β, while the flow was fully developed for large β.

In the entrance region ($\xi = 5.7$) the void fraction tended to be maximum at the wall (Figure 1) at moderate volumetric gas flow concentrations. As β increased, however, the maximum moved to the pipe center at this position (Figure 2), indicating that the length of the entrance region decreased with increasing β. In every case, however, an interesting inversion in the void fraction profile occurred as the flow became fully developed. The local liquid velocity exhibited a somewhat similar inversion (Figure 3). Relatively large fluctuations in pressure (1 to 5 in. Hg) were measured at the inlet mixing tee, attributed to the collapse of the slug undersurface due to Taylor instability. The profile measurements in the entrance region indicate that fluid entered principally near the walls, the returning fluid pouring down near the center. These effects might be considerably smaller with a well-dispersed inlet flow.

Void distributions very similar to these, with a maximum at the wall, were reported by Zivi and Wright (*15*) and Christensen (*16*) for subcooled boiling entrance regions, with a similar inversion of the profiles when the saturated boiling region was reached. That such dissimilar systems should show parallel behavior is quite worthy of note. The mercury-nitrogen flow system involved no gen-

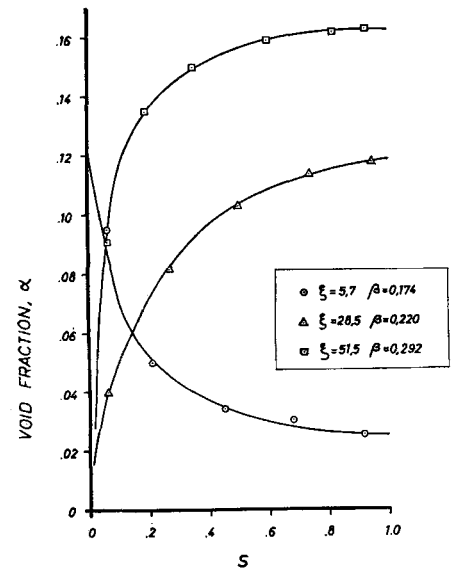

Fig. 1. Void fraction as a function of radial distance for different axial positions.

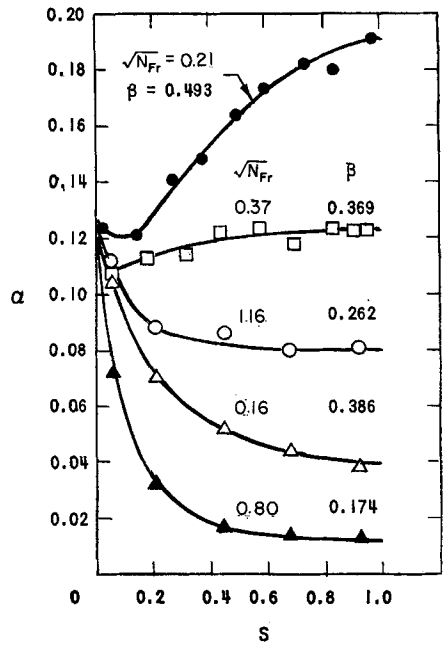

Fig. 2. Void fraction radial profiles in the entrance region for different gas volumetric flow concentrations.

eration of the vapor at the walls; owing to the strong nonwetting tendency of the mercury, the flow, even in the entrance region, is believed to have consisted largely of asymmetric slugs of mercury and gas, and the flow cross section was axisymmetric. On the other hand, in the boiling water experiments vapor was generated at the walls and because of the narrow rectangular cross section tended to concentrate first in the rectangular corners. No slug flow is possible in subcooled boiling water entrance regions, and the wetting properties of water for ordinary

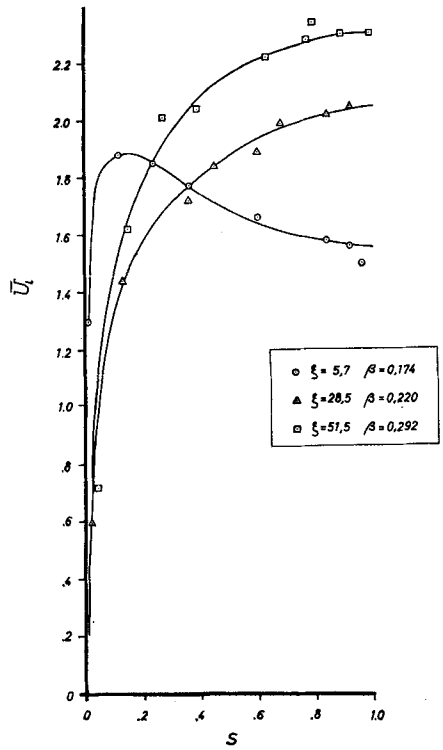

Fig. 3. Time-averaged local liquid velocity profiles at several axial positions.

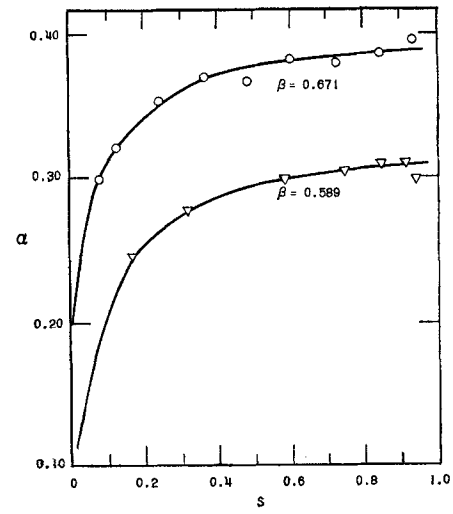

Fig. 4. Void fraction profiles at $\xi = 28.5$ and 51.5 in fully developed flow; $N_{Fr} = 0.044$.

stainless steel surfaces are greatly superior to those of mercury. From the marked dissimilarities of these flows, therefore, it would appear that the mean radial concentration and velocity profiles are dictated more by hydrodynamic considerations, possibly resulting from requirements for minimum energy dissipation in the total flow (*17*) than from surface wetting effects.

In fully developed flow, the void fraction profiles are, in some respects, similar to those in air-water or steam-water flows. Thus the curve is displaced upwards, with little change in shape, as the volumetric flow concentration β increases (Figure 4) at constant N_{Fr}. On the other hand, as the Froude number, based upon the superficial liquid velocity, is increased at constant β, the void fraction curves are also displaced upwards, showing that the Armand parameter $C = \alpha/\beta$ exhibits here a strong dependence upon mass velocity (Figure 5). Similarly, the liquid velocity profile is displaced upwards as β increases, both in the entrance region (Figure 6) and in fully-developed flow (Figure 7).

The profile data were plotted on semi-log paper and values of n and p found by drawing the best straight line through the data points. Table 1 was then constructed from Equations (27) to (29) for all the experiments in which both the void and velocity profiles were measured. Many other runs were made in which only the void profiles were measured; these data were also used to obtain the correlations to follow. The complete data for all ex-

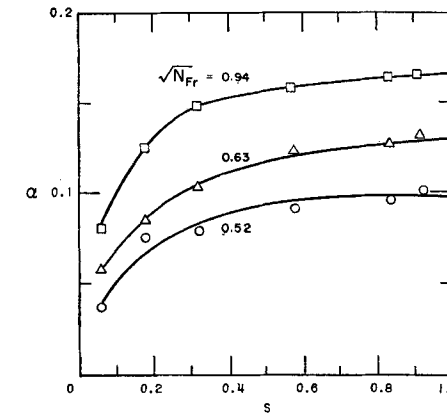

Fig. 5. Void fraction profiles at $\xi = 28.5$ and 51.5 for various Froude numbers; $\beta = 0.3$.

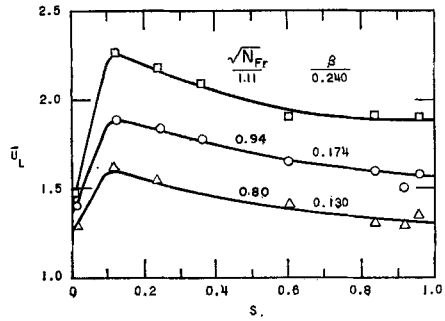

Fig. 6. Liquid velocity profiles at $\xi = 5.7$.

periments are available in tabular form in reference *18*. It is seen that the local slip φ far outweighs the distributional slip λ in this case, as might be expected. Also, the velocity and void fraction profiles are nearly flat, in view of the flow regime (slug) and the nonwetting characteristics of the mercury.

The functional dependence of the exponents n and p upon the flow parameters was found by fitting the data, with the method of least squares, to a three-constant equation to obtain

$$n = 15\left[\frac{\beta}{\sqrt{N_{Fr}}}\right]^{0.32} \tag{45}$$

$$p = 15\left[\frac{\beta}{\sqrt{N_{Fr}}}\right]^{0.25} \tag{46}$$

To within two significant figures, these exponents turn out to be functions of a single parameter $(\beta/\sqrt{Fr_o})$. The error in these equations is, however, estimated to be of the order of $\pm$ 20% for large values of the parameter, corresponding to very flat profiles. This, however, leads to a much smaller error in the distribution, for the same reason. These equations show that the more gas present, the more uniform is the distribution of both the gas fraction and liquid velocity, and as the total mass flow rate, which is essentially the mass flow rate of mercury, increases, the gas tends to become more concentrated at the tube center.

A least-squares program was also used to establish a flow-concentration relationship of the form

$$C = 1.25\,\beta^{0.88}N_{Fr}^{0.20} \tag{47}$$

with an estimated error of $\pm$ 5%.

Although velocity and void fraction profiles have not been previously determined for liquid metal flows, some investigations of the flow-concentration relationship have been made for boiling liquid metal systems. The principal data are from Gremilov (*19*), Siryi (*20*), and Korniev (*21*), as reported by Kutateladze et al. (*22*), and from Smith, Tang, and Walker (*23*). In all cases, the liquid metal was mercury or mercury amalgam. The Russian data covered the range of Froude numbers from 1 to 10, while the Smith et al. data were taken in an essentially noncirculating system ($N_{Fr} = 10^{-4}$). The curve of $\hat{\alpha}$ vs. β for constant N_{Fr}, calculated in accordance with Equation (47), was plotted in Figure 8 along with data for $N_{Fr} = 1.0 \pm 0.3$ and 0.01 ± 0.003. The dashed curves signify the boiling mercury data of Gremilov and Smith et al. It can be seen that the curve of Gremilov represents the data of this study very well.

On the other hand, Smissaert (*25*) has recently found slip ratios to be significantly higher for a mercury-nitrogen flow in a nickel-plated (presumably well wetted) test section than in the present study. A direct comparison cannot be made, since void fraction or velocity profiles were not measured. Nevertheless, a reasonable explanation seems to be that the gas concentrated more strongly near the center of the well-wetted section, so that distributional slip, in addition to local slip, played a significant role. Also, Baroczy (*26*) has recently generalized the Martinelli (*27*) correlation over a wide range of gas-liquid flows, including the horizontal mercury-nitrogen flow data in a 0.394 in. glass tube obtained by Kiraly and Koestel (*28*).

Table 1. Calculated Profile Data

β	N_{Fr}	n	p	Φ	λ	η
0.332	0.49	20	8.2	2.42	1.01	2.44
0.407	0.49	8.7	11.6	1.80	1.00	1.80
0.310	0.41	13.0	8.7	3.05	1.01	3.08
0.395	0.41	13.0	15.0	2.13	1.00	2.13
0.299	0.29	10.0	9.7	3.57	1.02	3.64
0.354	0.29	12.0	19.1	3.31	1.00	3.31
0.319	1.41	8.5	7.9	2.28	1.00	2.28
0.397	1.41	11.0	7.6	1.77	1.02	1.80
0.262	1.18	10.0	8.2	2.39	1.02	2.42
0.344	1.18	11.0	16.5	1.90	1.01	1.92
0.220	0.91	8.5	6.7	2.68	1.02	2.73
0.292	0.91	10.0	11.9	2.35	1.02	2.40
0.168	0.68	9.0	14.0	3.50	1.01	3.52
0.230	0.68	8.5	9.4	2.55	1.01	2.58
0.296	1.28	8.0	6.7	2.54	1.02	2.59
0.380	1.28	11.0	7.9	2.20	1.02	2.25

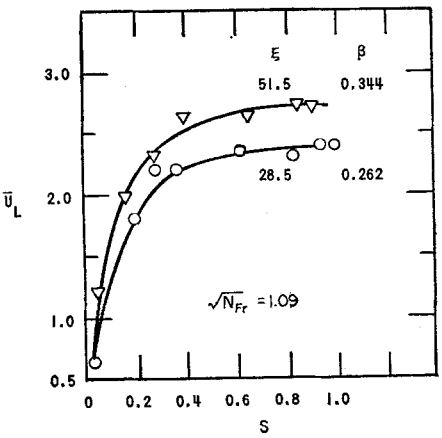

Fig. 7. Liquid velocity profiles at $\xi = 28.5$ and 51.5; $N_{Fr} = 1.2$.

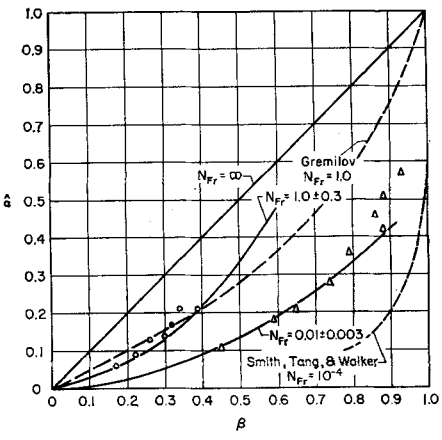

Fig. 8. Comparison of cross-sectional average void fraction vs. β for present work at two Froude numbers with data of Gremilov (19) and Smith, Tang, and Walker (23).

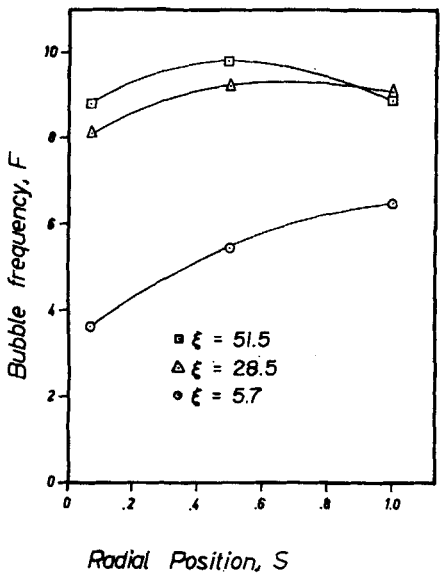

Fig. 9. Mean bubble frequencies vs. radial position; $N_{Fr} = 0.045$.

Bubble Parameters

The preceding correlations are useful in expressing in compact form the gross relationships between the system parameters, but they do not provide much insight into the physical mechanism. One observes that the velocity and void fraction profiles are both quite flat, which is a characteristic of slug flow. This is confirmed by measurements of bubble frequencies and bubble size distributions made with the resistivity probe described earlier (*1*). Some typical data are shown here, sampled from a large body of measurements (*18*).

Typical bubble frequencies are shown in Figure 9. The frequency of bubbles is fairly uniform across the channel cross section and does not change significantly as the stream proceeds up the tube. The latter result implies no net bubble coalescence, which in turn indicates a fully developed slug flow in only 28.5 pipe diameters.

Typical bubble size distribution data* for the entrance region are given in Figure 10 and for fully developed flow in Figure 11. These data show that the bubble-size distribution varies considerably with radial position at $\xi = 5.7$, with more small bubbles near the wall, but when the slug flow is fully developed, differences in the distribution function become almost indistinguishable. Over 99% of the gas flow is contained in bubbles whose length is equal to or greater than the pipe diameter. This is, therefore, a highly segregated slug flow, illustrative of the well-known coalescing tendency of gas bubbles in liquid metals.

It might be inferred from the flat velocity and void fraction profiles, and the relative independence of bubble frequency upon radial position, that this was a slug flow quite similar to those studied in aqueous systems by Griffith and Wallis (*29*), Griffith and Moissis (*30*), and Nicklin, Wilkes, and Davidson (*31*). This is, however, not at all the case, as was shown by a study of gas slugs rising through a stationary mercury column in a one inch glass tube.† The gas slugs were no longer symmetrically centered in the tube as in air-water flow but hugged one wall of the tube. Slugs less than about 4 in. long were oriented essentially vertically but tended to rotate in position around the tube wall as they rose. Mercury poured past the flood in an asymmetric manner. Hence the analysis given by Davies and Taylor (*32*) for axisymmetric bubbles and modified by Griffith and Wallis (*29*) and Wallis (*33*) requires modification. The original analysis was based upon the concept of inviscid flow past a free cavity and hence led to the Froude number as the only significant independent variable. Although it seems probable that viscous forces can be neglected also in the mercury-nitrogen system, it is not at all clear that interfacial drag forces exerted by the wall on the gas bubbles will be negligible.

For longer slugs the situation was even more complicated. The slug tended to assume a helical shape along the inside of the pipe, so that a definite swirl was imparted to the two-phase flow. A similar phenomenon is frequently seen in the drainage of water from a greasy tube. It should be noted that the photographs were taken in a mercury stand tube, corresponding to zero inlet velocity, and hence zero Froude number. The necessity for the total volumetric flow range to be zero at every axial position made it very difficult to sustain a gas slug which filled the entire cross section. This is a basic difference between wetting and nonwetting slug flows. In wetting flows, liquid drains past the slugs close to the

* The bubble size corresponding to a particular time interval τ during which the bubble is in contact with the probe tip is determined by assuming that the bubble travels at the local gas velocity, and that the mean bubble diameter is identified with the median diameter. Since neither assumption is strictly correct, these plots should be considered to be indicative of the relative bubble distribution. More sophisticated methods for caculating the mean bubble diameter are discussed in communications to this journal by Anderson (*34*) and by Bankoff (*35*).

† Note the assumption, which may not be valid, that the behavior in the glass standpipe was similar to that in the stainless steel loop.

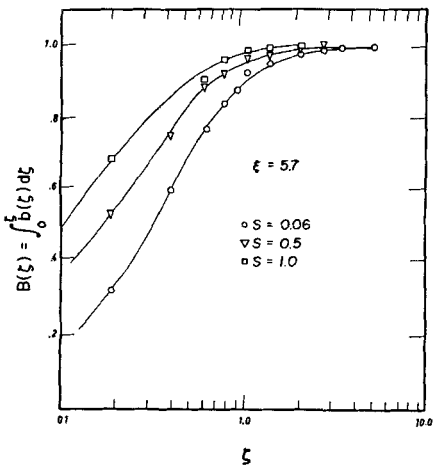

Fig. 10. Bubble diameter distribution near the entrance of test section; $N_{Fr} = 0.045$ and $\beta = 0.51$.

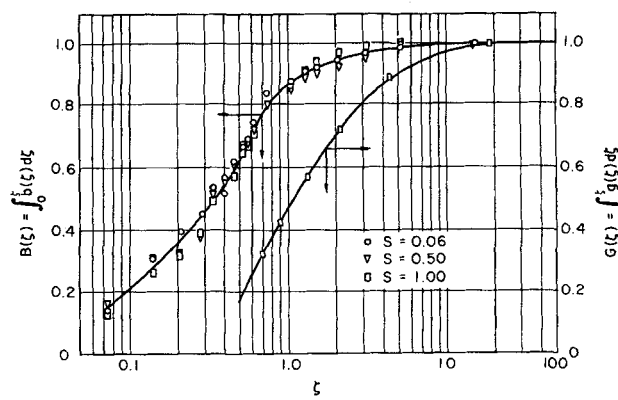

Fig. 11. Bubble diameter and gas slug length distributions in fully developed flow; $N_{Fr} = 0.045$.

walls at any Froude number. But in nonwetting flows, gas slugs which occupy the entire cross section do not permit drainage of liquid past them and hence are inherently unstable at slip velocity ratios greater than 1. In a stand tube, the slip velocity ratio is, of course, infinite, but even in circulating flows, it is seen from Table 1 that the slip velocity ratio is greater than 2. For this reason a cross-sectional slug, if it forms, can lift the mercury above it only a short distance before it becomes unstable. This might account for some of the observed pressure oscillations, especially those associated with the entrance conditions.

According to Griffith and Moissis (*30*), the annular wake behind a slug in a developing flow causes the nose of the following slug to rise more rapidly, eventually resulting in agglomeration. In this work, however, the picture is considerably different. It is probable that individual slugs are positioned asymmetrically, so that the tendency for slugs to attract one another induces a rotatory component to the flow. The fact that the bubble frequency is essentially the same at all radial positions indicates that the small bubbles interspersed with the liquid mercury streaming past the slugs do not concentrate near the wall and that most gas slugs extend inwards at least as far as the center of the tube.

Griffith has recently presented a correlation (*24*) for prediction of void fractions in fully developed slug flows. He begins with the continuity expression developed by Griffith and Wallis (*29*) for this type of flow

$$\hat{\alpha} = \frac{Q_G}{Q_L + Q_G + U_b A} = \frac{1}{\frac{1}{\beta} + \frac{U_b}{\hat{U}_{SG}}} \tag{48}$$

where U_b is the rise velocity of the slug with reference to the liquid far in front of it, and the superficial gas velocity is defined by

$$\hat{U}_{SG} = \hat{U}_G (1 - \alpha) \tag{49}$$

From a continuity balance one obtains

$$\varphi = \frac{\hat{U}_G}{\hat{U}_L} = \frac{1 - \hat{\alpha}}{\hat{\alpha}\left(\frac{1}{\beta} - 1\right)} \tag{50}$$

It is readily shown that this expression applies to any two-phase flow, providing one takes the bubble rise velocity to be equal to the gas velocity relative to that of the mixture

$$U_b = \hat{U}_G - \hat{U}_M \tag{51}$$

where

$$U_M = \frac{Q_L + Q_G}{A} \tag{52}$$

$$= \hat{U}_L(1 - \alpha) + \hat{U}_G(\alpha) \tag{53}$$

The void fraction can therefore be predicted providing the bubble rise velocity or relative gas velocity is known. The expression given by Griffith is

$$U_b = K_1 K_3 \sqrt{gD_b} + K_2 \left(\frac{Q_L + Q_G}{A}\right) \tag{54}$$

where K_1 is an empirical proportionality constant determined from a tube emptying experiment, K_3 is a factor which takes into account the difference in bubble rise velocity in heated and unheated sections and is unity for an unheated section, and K_2 is interpreted by Griffith to be the proportion that the liquid immediately ahead of the slug moves faster than the mixture velocity. Nicklin, Wilkes, and Davidson found in an air-water atmospheric pressure flow (*31*) that $K_2 = 0.2$ for $Re > 8{,}000$. Choosing the center-line liquid velocity as the maximum velocity of the liquid ahead of the slug, one obtains

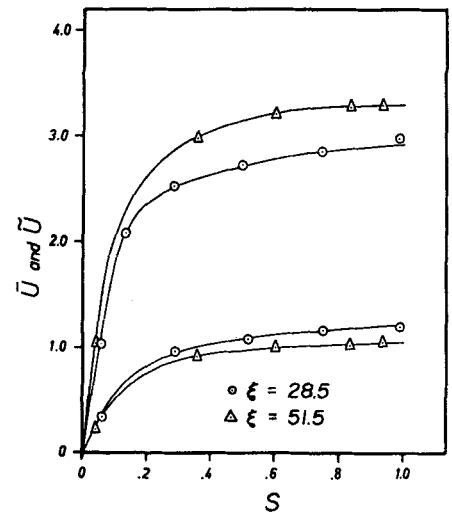

Fig. 12. Mean and standard deviation of the stream velocity, ft./sec., vs. radial position; circle with dot $\xi = 28.5$ and triangle with dot $\xi = 51.5$. $N_{Fr} = 1.2$.

$$K_2 \leq U_{Lo}/\hat{U}_L - 1 \tag{55}$$

It can readily be shown from Equation (27) that

$$K_2 \leq \frac{1}{\Omega_n} - 1 = \frac{3n + 1}{2n^2} \tag{56}$$

As pointed out by Griffith, $K_2 = 0.2$ corresponds to $n = 7.8$. Reference to Table 1, however, shows that the liquid velocity exponent n in mercury-nitrogen flow has a range of variation of about 8 to 20, with a mean, excluding the one value of 20 (which may have been a still developing flow) of 10.1, corresponding to $K_2 \leq 0.15$. This is a reflection of the flatter velocity profiles in nonwetted-wall flows.

Fluctuating Characteristics of the Two-Phase Stream

In Figures 12 and 13 are given typical plots of mean liquid velocity and stream density, as well as root-mean-

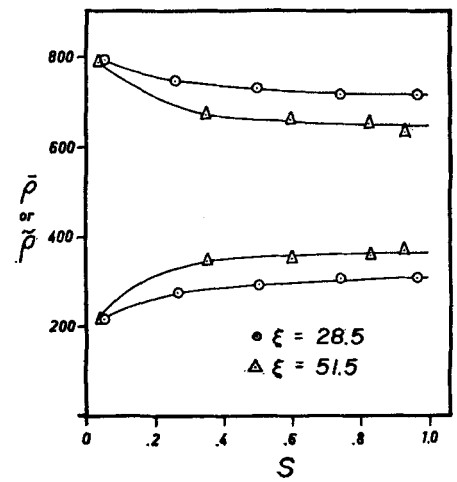

Fig. 13. Mean and standard deviation of stream density vs. radial position; conditions same as in Figure 12.

square values of the fluctuation of these quantities from their mean values, as a function of radial position at two axial locations. It was observed once more that the flow was reasonably developed at 28.5 pipe diameters from the entrance, and the velocity and void fraction profiles were quite flat. The root-mean-square measurements are believed to be the first of their kind to be reported. The intensities of the mixture velocity and density fluctuations are not small, as in the usual single-phase turbulent flow, but range from 20 to 50% of the mean stream property. Levy (3) assumes in his mixing-length theory that both $\tilde{\rho}/\rho$ and $\tilde{u}/u << 1$, which is not borne out by these measurements. These intensities may be smaller in aqueous two-phase flow, since from Equations (19) and (20) the fluctuating quantities become larger as the void fraction approaches 0.5, the local buoyant slip φ becomes large, and/or as the density ratio γ becomes small.

Levy (3) defines a density mixing length and a velocity mixing length by the equations

$$l_u = \tilde{u} \left| \frac{dy}{d\overline{U}} \right|; \quad l_\rho = \tilde{\rho} \left| \frac{dy}{d\rho} \right| \qquad (57)$$

and assumes that $l_u = l_\rho = cy$, where c is a constant. The development of the resistivity probe for local void-fraction measurement and the momentum probe for local liquid velocity makes it possible to test the validity of these assumptions. The mixing length as defined by these equations were calculated for ten runs by numerically differentiating the mean velocity and density profiles. The results at two axial locations for four typical runs are shown in Figures 14 and 15, where the ordinate represents the dimensionless mixing lengths as a function of dimensionless distance from the wall. It is seen that the density mixing lengths are several times greater than the corresponding velocity mixing lengths. Despite the relatively large uncertainty in l_u and l_ρ near the pipe axis, owing to the nearly flat profiles in this region, it is evident that a linear relationship between the mixing lengths and S does not hold over the entire flow region. Close to

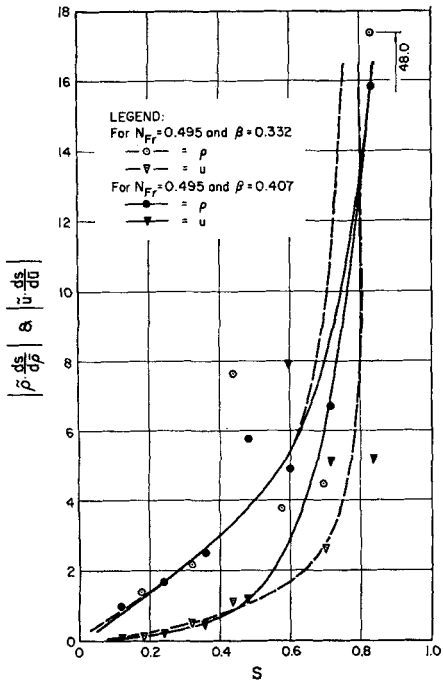

Fig. 14. Mixing lengths for velocity and density transport.

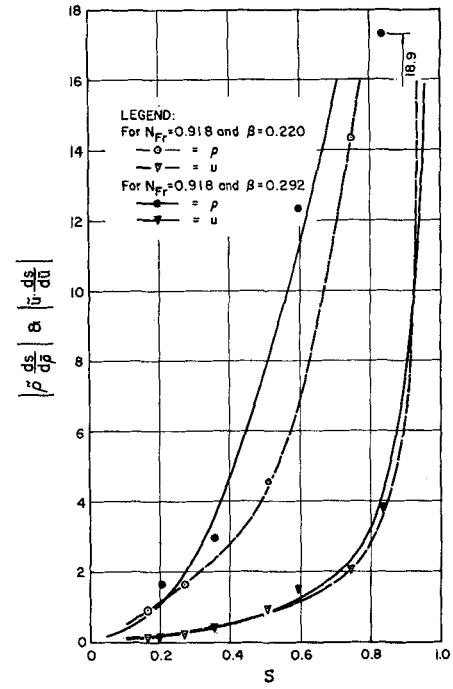

Fig. 15. Mixing lengths for velocity and density transport.

the wall a linear approximation seems reasonable, but in this case the slopes are quite different for the velocity and density mixing-length curves. Furthermore, the mixing lengths obtained from Figures 14 and 15 are unrealistically large, being of the order of the pipe diameter. As might be expected from the highly segregated nature of the flow, one concludes that the present mixing-length theory is not applicable to liquid metal-gas flow with unwetted walls. One reason may be that the theory makes no distinction between fluctuations in velocity and density caused by radial transport of mass or momentum and those resulting from the alternation of liquid and gas at a particular point in the flow. This would seem to be necessary, since the latter contribution, which is not associated with radial transport, is the dominant one in the present study. It might be thought that this difficulty can be circumvented by employing an expected-value operator such that the time averaging is performed over some volume of fluid surrounding the point, corresponding to one of the lumps visualized by Prandtl. However, such an averaging procedure would diminish contributions from both mechanisms approximately equally, leaving the gas-liquid alternation as the dominant contribution. Furthermore, if the radial mixing length is of the same order as the mixing length in the corresponding single-phase flow at the same total Reynolds number, the diameter of these lumps would be less than 0.1 in., which is the limit of resolution of the resistivity probe for bubble detection. Hence, a time average over a lump of this size would be equivalent to averages taken at a single point, which is the expected-value operation implied in the Prandtl single-phase mixing-length theory. Finally, the need for measurements of turbulent radial mass fluxes in two-phase flow, which are not presently available, is pointed up by this study.

ACKNOWLEDGMENT

The experimental work described herein was performed at Argonne National Laboratory under the auspices of the Atomic Energy Commission under a cooperative arrangement with Northwestern University through the Associated Midwest

Universities. Particular thanks are due to Dr. P. A. Lottes and Mr. Albert Stogsdill of Argonne National Laboratory, and Dr. Helge Christensen, of the Institutt for Atomenergi, Kjeller, Norway.

An important portion of the theoretical work was supported by a grant from the National Science Foundation.

NOTATION

A = cross-sectional area
$B(\zeta)$ = fraction of bubbles with dimensionless diameter less than ζ
$b(\zeta)$ = bubble diameter probability density, equal to $dB(\zeta)/d\zeta$
C = Armand constant, Equation (41)
C_1 = calibration constant
D = diameter
E = expected-value operator
F = bubble frequency
N_{Fr} = Froude number, $\bar{U}_{SL}^2/gD_p$
$G(\zeta)$ = fraction of gas slugs whose dimensional length is less than ζ
K, K_1, K_2, K_3 = constants defined by Equations (39) and (54)
L = integration length
l_u, l_ρ = velocity and density mixing lengths
m, n, p = exponents defined by Equations (27), (28), (29)
N = number of bubbles
P = probability or pressure
Q = volumetric flow rate
R = region of integration or pipe radius
$\mathbf{r}$ = radius vector
S = dimensionless distance from wall
T = time interval
t = time
$\mathbf{U}$ = velocity vector
V = volume
x = quality
$X(\mathbf{x}, t)$ = stochastic variable, equal to 0 or 1, depending upon whether gas or liquid present at the point in space time
y = distance from wall
z = axial distance

Greek Letters

α = time-average local void fraction
β = volumetric gas flow concentration, $Q_G/(Q_L + Q_G)$
γ = ρ_G/ρ_L
δ = Ω_{mp}/Ω_{pn}
ζ = space-average instantaneous void fraction; also bubble diameter or slug length made dimensionless with respect to pipe diameter
η = $\hat{U}_G/\hat{U}_L$
θ = angle of deflection of flow by impact probe
ξ = dimensionless axial distance, z/D_p
ρ = density
φ = $\bar{U}_{Go}/\bar{U}_{Lo}$
Ω_p, Ω_{mp} = constants defined by Equations (33), (34)

Subscripts

b = bubble
G = gas
L = liquid
p = pipe
S = superficial
t = time
x_1 = average along x_1 direction
o = center line, or maximum

Superscripts

$-$ = time average
$\wedge$ = cross-sectional average
$'$ = instantaneous fluctuation
$\sim$ = root-mean-square value of fluctuations

Other Symbols

$\langle\rangle$ = space-average

LITERATURE CITED

1. Neal, L. G., and S. G. Bankoff, *A.I.Ch.E. Journal*, **9**, 490 (1963).
2. Bankoff, S. G., *J. Heat Transfer, Trans. Am. Soc. Mech. Engrs.*, **82C**, 265 (1960).
3. Levy, S., *ibid.*, **85C**, 137 (1963).
4. Hudson, J. L., K. M. Atit, and S. G. Bankoff, *Chem. Eng. Sci.*, **19**, 387 (1964).
5. Lighthill, M. J., and G. B. Whitham, *Proc. Roy. Soc.*, **A229**, 281, 317 (1955).
6. Zuber, N., and J. Hench, *Rept. 62GL100*, General Electric Co., Schenectady, New York (1962).
7. Wallis, G. B., *AERE R162*, Atomic Energy Establishment, Harwell, England.
8. Armand, A. A., *Izvestia VTI*, **1**, 16 (1946).
9. ———, and G. G. Treschev, *ibid.*, **4**, 1 (1947).
10. Zuber, N., *J. Heat Transfer, Trans. Am. Soc. Mech. Engrs.*, **82C**, 255 (1960).
11. Hughmark, G. A., *Chem. Eng. Progr.*, **58**, 62 (1962).
12. ———, and B. S. Pressburg, *A.I.Ch.E. Journal*, **7**, 677 (1961).
13. Jones, A. B., *KAPL-2170*, General Electric Co., Schenectady, New York (1961).
14. ———, and D. G. Digt, *KAPL-2208*, General Electric Co., Schenectady, New York (1962).
15. Wright, R. W., et al., *STL-6112*, Space Technology Laboratories, Inc., Redondo Beach, California (1961).
16. Christensen, H., *ANL-6385*, Argonne National Laboratory, Argonne, Illinois (1961).
17. Zivi, S. M., *STL-6212*, Part IV, Space Technology Laboratories, Inc., Redondo Beach, California (1962).
18. Neal, L. G., Ph.D. thesis, Northwestern Univ., Evanston, Illinois; also *ANL-6625*, Argonne National Laboratory, Argonne, Illinois (1963).
19. Gremilov, D. I., *Trudy Ts KTI, Mashgiz, Leningrad*, **23**, 44 (1952).
20. Siryi, P. O., et al., *Sovetskoe Kotloturbostroenie*, **8-9**, 375 (1938).
21. Korniev, M. I., *Teploenergetika*, **4**, 44 (1955).
22. Kutateladze, S. S., V. M. Borishanskii, and I. I. Novikov, *J. Nucl. Energy II*, **9**, 214 (1959).
23. Smith, C. R., Y. S. Tang, and C. L. Walker, *A.I.Ch.E. Journal*, **10**, 586 (1964).
24. Griffith, P., *J. Heat Transfer, Trans. Am. Soc. Mech. Engrs.*, **86C**, 327 (1964).
25. Smissaert, G. E., *ANL-6755*, Argonne National Laboratory, Argonne, Illinois (1963).
26. Baroczy, C. J., A.I.Ch.E. Preprint No. 26, 6th Natl. Heat Transfer Conference, Boston, Mass. (1963).
27. Lockhart, R. W., and R. C. Martinelli, *Chem. Eng. Progr.*, **45**, 39 (1949).
28. Kiraly, R., and A. Koestel, *Report No. ER-4104*, Thompson-Ramo-Wooldridge Corp., Cleveland, Ohio (1960).
29. Griffith, P., and G. B. Wallis, *J. Heat Transfer, Trans. Am. Soc. Mech. Engrs.*, **83C**, 307 (1961).
30. ———, and R. Moissis, *ibid.*, **84C**, 29 (1962).
31. Nicklin, D. J., J. O. Wilkes, and J. F. Davidson, *Trans. Inst. Chem. Engrs.*, **40**, 61 (1962).
32. Davies, R. M., and G. I. Taylor, *Proc. Roy. Soc. London*, **200A**, 375 (1950).
33. Wallis, G. B., *Rept. No. 62GL130*, General Engineering Laboratory, General Electric Co., Schenectady, New York (1962).
34. Anderson, T. T., *A.I.Ch.E. Journal*, **10**, 776 (1964).
35. Bankoff, S. G., *ibid.*

Manuscript received June 24, 1964; revision received December 30, 1964; paper accepted January 13, 1965.